

Article

Permeability Evolution of Porous Sandstone in the Initial Period of Oil Production: Comparison of Well Test and Coreflooding Data

Mikhail S. Turbakov ¹, Evgenii V. Kozhevnikov ^{1,*}, Evgenii P. Riabokon ¹, Evgeniy A. Gladkikh ¹, Vladimir V. Poplygin ¹, Mikhail A. Guzev ² and Hongwen Jing ³

¹ Department of Oil and Gas Technologies, Perm National Research Polytechnic University, 614990 Perm, Russia

² Institute of Applied Mathematics, Far Eastern Branch of the Russian Academy of Sciences, 690950 Vladivostok, Russia

³ State Key Laboratory for Geomechanics and Deep Underground Engineering, China University of Mining and Technology, Xuzhou 221116, China

* Correspondence: kozhevnikov_evgen@mail.ru

Abstract: Permeability prediction in hydrocarbon production is an important task. The decrease in permeability due to depletion leads to an increase in the time of oil or gas production. Permeability models usually are obtained by various methods, including coreflooding and the field testing of wells. The results of previous studies have shown that permeability has a power-law or exponential dependence on effective pressure; however, the difficulty in predicting permeability is associated with hysteresis, the causes of which remain not fully understood. To model permeability, as well as explain the causes of hysteresis, some authors have used mechanical reservoir models. Studies have shown that these models cannot be applied with small fluctuations in effective pressures in the initial period of hydrocarbon production. In this work, based on the analysis of well test data, we came to the conclusion that in the initial period of production under constant thermobaric conditions, the permeability of a slightly clayey terrigenous reservoir depends on the amount of fluid produced. A model has been obtained that describes the change in permeability in the initial period of oil production. Core samples were flooded to confirm the model. Coreflooding showed high convergence of the model obtained from well test data. With computed tomography (CT) and scanning electron microscope (SEM), the properties and structure of the core were studied, and it was found that the main reason for the decrease in the permeability of slightly clayey rocks in the initial period of production is the migration of natural colloids.

Keywords: permeability; permeability hysteresis; colloid migration; coreflooding; porous media



Citation: Turbakov, M.S.; Kozhevnikov, E.V.; Riabokon, E.P.; Gladkikh, E.A.; Poplygin, V.V.; Guzev, M.A.; Jing, H. Permeability Evolution of Porous Sandstone in the Initial Period of Oil Production: Comparison of Well Test and Coreflooding Data. *Energies* **2022**, *15*, 6137. <https://doi.org/10.3390/en15176137>

Academic Editor: Hossein Hamidi

Received: 6 July 2022

Accepted: 22 August 2022

Published: 24 August 2022

Publisher's Note: MDPI stays neutral with regard to jurisdictional claims in published maps and institutional affiliations.



Copyright: © 2022 by the authors. Licensee MDPI, Basel, Switzerland. This article is an open access article distributed under the terms and conditions of the Creative Commons Attribution (CC BY) license (<https://creativecommons.org/licenses/by/4.0/>).

1. Introduction

When hydrocarbons are produced or water is injected, the pore pressure and effective Terzaghi pressure (P_{eff}) change, the reservoirs are deformed and their permeability changes [1–4]. Permeability modeling during reservoir depletion becomes especially important in hydrocarbon production forecasting. The change in permeability from effective pressure is mainly determined in laboratory studies of core samples. In addition to laboratory studies, the sensitivity of permeability to effective pressure can be determined from well test data [5–7]. In both cases, researchers agree on the general conclusion that permeability is a power-law or exponential function of effective pressure (Figure 1) [6,8,9].

Despite the widespread use of laboratory flooding methods, the results of laboratory studies may not be sufficient to describe the properties of real reservoirs. Studies [6,9] have shown that the sensitivity of permeability to effective pressure, determined by well testing, is higher than that determined in the laboratory for the following reasons:

- the permeability determined during well testing takes into account the zonal and layered heterogeneity of the oil reservoirs;
- formation pressure change leads to formation deformation, fracture closure and separation of individual layers;
- during extraction, the core undergoes significant volumetric deformations and can no longer reflect natural conditions.

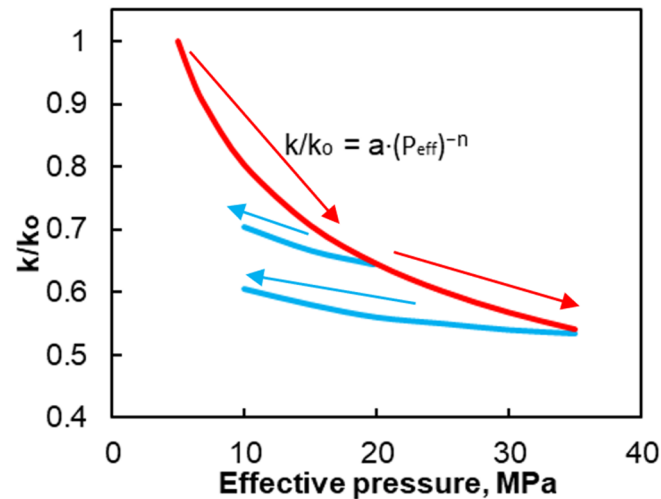


Figure 1. Influence of effective pressure on the relative permeability of rocks. The red arrows show the loading stage, the blue—unloading.

Moreover, in some works [10–13], it is noted that with a cyclic change in the effective pressure, a permeability hysteresis is observed—its incomplete recovery when the effective pressure returns to the initial state. The permeability hysteresis does not depend on the type of rock, porosity, fracturing, and the nature of the change in effective pressure (due to pore pressure or rock pressure) [12,13]. The complexity and presence of a large number of factors affecting permeability make research on its prediction quite relevant.

Some researchers use mechanical models to predict permeability from effective pressure. In [2,14], the nonlinear change in the permeability of rocks under loading (increase in P_{eff}) is described by representing a poroelastic medium as a Two-part Hook's Model (TPHM), consisting of two springs—a hard spring and a soft spring (Figure 2a). A hard spring corresponds to the true elasticity of the rock, and a soft spring characterizes the compression of micropores and microcracks during initial compaction. Both springs experience the same stress, but their deformation occurs according to different laws. An example of using the TPHM model is presented in [14], where, based on laboratory data from [2], modeling and verification of the results were carried out. Mathematically, the hard and soft parts of the TPHM model can be described by exponential, power, and linear equations. The TPHM model describes the nonlinearity of the change in permeability, but does not characterize the presence of hysteresis, since it is elastic.

Natural rocks, including porous ones, have viscoelasticity and permanent deformation caused by plastic deformation or compaction. In rocks, even a slight change in the effective pressure in the zone of elastic loading can lead to creep, which is characterized by an increase in deformation at constant stress. The authors of [15] presented a mechanical model that takes into account the effect of rock creep. The model (Figure 2c) consists of two main parts—elastic (linear) and viscoelastic (nonlinear)—and is based on the exponential equation of permeability from effective pressure. Obviously, such a model can only be used in those rocks in which the content of plastic particles, such as clays, exceeds certain values; however, many researchers believe that creep is the main cause of permeability hysteresis in any type of rock.

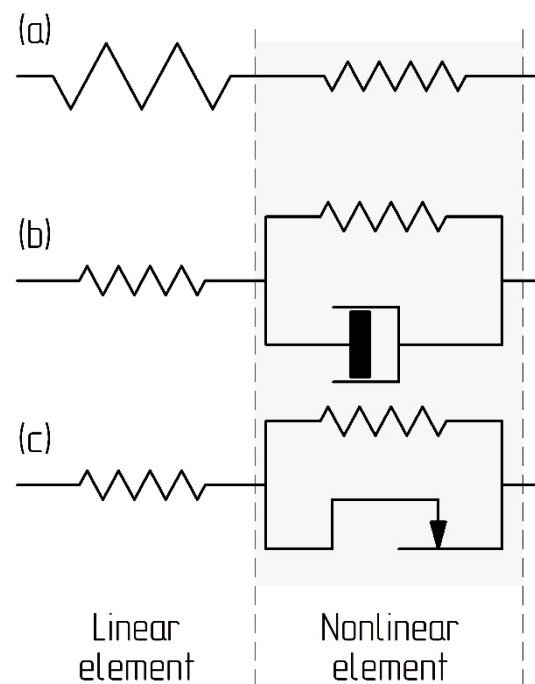


Figure 2. Models describing the nonlinearity of permeability as a function of effective pressure: (a) TPHM; (b) model with friction element; (c) model with viscous element.

With creep, the decrease in permeability is a consequence of the decrease in porosity. Then, in porous media with a rigid matrix, creep should not affect porosity and permeability; in support of this, the authors of [16] conclude that in sandstones with a clay content of up to 10%, porosity does not change when samples are loaded, even at an effective pressure of more than 50 MPa. In [17], laboratory studies of Vosges sandstone showed that when loading and unloading sandstone samples with a maximum effective pressure of 36 MPa, the decrease in porosity was 0.3%, and the permeability decreased by 6.7 times. Computed tomography [18] showed that microcracks close under load, while the size and shape of the pores do not change. Based on this, the authors conclude that in weakly clayey porous rocks, pore compression and creep are not the main cause of permeability hysteresis, and the main decrease in permeability occurs due to the closure of microcracks. Similar conclusions that the permeability of rocks is mainly due to the presence of microcracks, which are more compressible than pores, are indicated in [19,20].

In [21], the permeability hysteresis is explained by the incomplete opening of a macrocrack. In this regard, the permeability model includes a friction element (Figure 2b), which describes the threshold resistance to fracture opening. It is assumed that the right side of the model (Figure 2b) does not work under loading but takes part only in the unloading cycle. Studies [19] have shown that this approach can also be used for porous media in which microcracks are present.

The decrease in permeability due to the closure of microcracks occurs with a large change in effective pressure, from units to tens of MPa. In reservoir conditions, a large pressure change corresponds to almost complete depletion; however, analysis of data from oil fields in the Perm region showed that permeability hysteresis is also observed in the early stages of oil production with a smaller reservoir pressure fluctuation. In this regard, the threshold model is not suitable for predicting permeability for small changes in effective pressures and does not describe the permeability hysteresis.

The purpose of this work is to establish the reasons for the decrease in permeability and its hysteresis, as well as to create a model for the permeability of terrigenous low-clay oil-bearing formations in the initial period of oil production with a slight decrease in reservoir pressure. Based on the analysis of well test data of the Perm region fields, as well as the results of coreflooding, we proposed a model for predicting the permeability

of porous low-clay media in the initial period of oil production, and also proposed a new explanation for the causes of permeability hysteresis.

2. Permeability Evolution Based on the Analysis of Well Test Data

In this work, we analyzed well test data at one of the oil fields in the north of the Perm region, which are located near the cities of Solikamsk and Berezniki (Figure 3). The oil fields of the region are represented by the same reservoirs with similar properties. In our work, we considered wells that exploited the C_{1tl} terrigenous reservoir, which is represented by low-clayey sandstones. Reservoir depth varies from 2030 to 2350 m, porosity—from 8 to 14%, permeability from 0.239 to 0.522 D. The initial pore pressure was 18 MPa.



Figure 3. Location of oil fields in the north of the Perm region. Source—OpenStreetMap, data is available under the Open Database License, openstreetmap.org/copyright.

From 1999 to 2020, more than 250 well tests were carried out at the considered field. In this work, the well test analysis was carried out for those wells in which the pore pressure decreased and increased during operation. To avoid the influence of relative phase permeability, the following criteria were also taken into account: reservoir pressure in the well area should not fall below saturation pressure during the operation period; water cut should not exceed 5%. Wax deposition under such thermobaric conditions is unlikely, so it can be neglected. A total of 20 wells was selected with 109 well tests corresponding to the given conditions.

For a comparative assessment, the permeability and effective pressure are given in a dimensionless form: k/k_o —relative permeability; P/P_o —relative effective pressure, k and P —measured during the production of the oil reservoir, permeability and effective pressure, respectively, low index o means initial pressure and permeability.

As a result of the well test analysis, a permeability hysteresis was established. Figure 4a shows a plot of permeability versus effective pressure for one of the wells. With a slight increase in effective pressure, the permeability quickly decreases and does not recover even with an increase in reservoir pressure above the initial one (Figure 4a). The same is observed in core studies [10–13]. Not all literary sources provide an exhaustive explanation of this phenomenon, and we also did not find data on the study of changes in the permeability of oil reservoirs with a cyclic change in effective pressure according to well test data.

Figure 4a shows that even with a slight change in effective pressure, the permeability in the initial period of production drops sharply and cannot be described by any mathematical equation, and the same is observed for other wells. The well test permeability model proposed in [5] shows how permeability changes with a decrease in reservoir pressure and cannot be used to predict permeability with an increase in reservoir pressure.

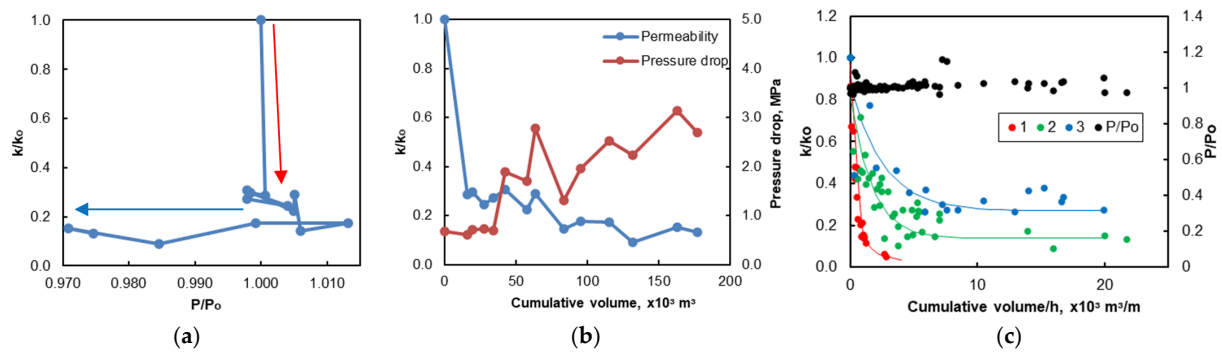


Figure 4. (a) Change in relative permeability on relative effective pressure. The red arrow shows the load stage, the blue arrow shows the unloading stage; (b) change in relative permeability and pressure drop on cumulative produced oil of one of the wells; (c) change in relative permeability and relative effective pressure on specific volume (cumulative produced oil divided by formation thickness) for 20 wells operating the C_{1tl} terrigenous formation. The circles show the actual values, the solid lines show the model values.

In the initial period of well operation, the decrease in effective pressure is insignificant; in our case, the maximum change in effective pressure in most wells does not exceed 5%—with such a small change in effective pressure, the decrease in permeability due to narrowing of pores and compression of microfractures is insignificant. It was found that the permeability depends on the amount of oil produced from the well (Figure 4b). Figure 4b shows that during production, the permeability decreases, and the pressure drop between the well and reservoir pressure increases. Figure 4 shows graphs of normalized permeability and effective pressure depending on the specific volume of produced fluid for 20 wells.

Figure 4a shows that with a slight change in effective pressure, the permeability decreases rapidly, the largest decrease occurs in the initial period of production. Permeability versus specific volume produced (Figure 4c) best fitted with the equation

$$\frac{k}{k_0} = a \cdot \text{Exp}(b \cdot V) + c \cdot V + d \quad (1)$$

where, a , b , c , d are coefficients determined using curve fitting analysis; V is the specific volume (cumulative produced oil divided by formation thickness) of fluid produced from the well before the well test.

According to the curve fitting analysis, the wells were divided into three groups, in which the decrease in permeability occurs with different intensity. It was not possible to establish the influence of well operating conditions and reservoir properties on the intensity of permeability reduction due to a large number of factors and their variability. For each group of wells, the coefficients of Equation (1) were calculated, the results are presented in Table 1.

Table 1. Reservoir and production data and calculated values of coefficients for Equation (1).

Group	1	2	3
Number of wells	5	8	7
k_0 , D	0.04–0.1	0.04–2.0	0.09–0.13
Maximum productivity, $\text{m}^3/(\text{d} \cdot \text{m} \cdot \text{MPa})$	0.18–1.75	0.21–9.5	0.9–1.1
ΔP , MPa	4.5–7.5	0.67–5.5	7.6–8.1
a	0.88	0.69	0.61
b	−2.31	−0.6	−0.39
c	−0.015	−0.008	0.0001
d	0.092	0.137	0.267
R^2	0.98	0.92	0.78

The decrease in permeability during production can occur for various reasons:

- narrowing of pores by increasing the effective pressure;

- deposition of organic and inorganic precipitations within pores;
- changes in relative phase permeability;
- migration of colloids.

Well test data selection criteria exclude the influence of some factors on the basis that:

- change in effective pressure in the observed wells did not exceed 5%, while the formation deformation should not be significant, which does not correspond to a decrease in permeability;
- deposition of organic and inorganic precipitations within pores did not occur because thermobaric conditions did not contribute to this. The temperature in the well does not change during production, and the bottomhole pressure in the well and in the reservoir does not drop below saturation pressure, so organic deposits and gas release are unlikely;
- scale precipitation is possible due to the interaction of incompatible waters. In our case, the water cut in the wells did not exceed 5%, so the effect of watered perforations is insignificant and cannot lead to large changes in permeability;
- there was no change in the relative phase permeability, since only oil enters the well under the selected conditions.

Excluding these factors, it remains that the most likely reason for the decrease in permeability and its hysteresis may be the migration of colloids. This hypothesis is also supported by the fact that permeability has a clear dependence on the amount of oil produced. To confirm this phenomenon, coreflooding tests were carried out, the results of which are presented in the next chapter.

3. Permeability Evolution Based on the Coreflooding Data

3.1. Rock Samples and Procedure

Four core samples of fine-coarse-grained siltstone from C₁tl terrigenous reservoir of the considered field were tested. Rock samples without chips, artificial cracks, and irregularities have a cylindrical shape with diameter of 30 mm and a length of 30 mm. Properties of core samples are shown in Table 2.

Table 2. Properties of core samples.

Sample №	1	2	3	4
Absolute permeability, D	0.9	47.27	52.12	27.97
Porosity, %	8.2	10.31	8.45	8.33

The structure of the pore space of the samples was assessed with computed tomography (CT) and scanning electron microscope (SEM) in atmospheric conditions before and after coreflooding. CT was used to verify the absence of cracks and the uniformity of the core properties, as well as to compare the change in the structure of the pore space before and after coreflooding. The SEM results showed the presence of a large amount of debris and colloids of various sizes and shapes (Figure 5). The presence of colloids can lead to a decrease in permeability during migration [21].

Before flooding, the samples have been cleaned of residual formation fluids and dried to constant weight.

Before flooding, samples were saturated with deionized water or kerosene under vacuum conditions for 24 h. The saturated sample was placed in a coreholder of coreflood apparatus—Auto Flood Reservoir Conditions Coreflooding System, AFS-300 production of Core Laboratories (Figure 6a). The pore pressure and confining pressure were gradually increased to the natural formation conditions at a temperature of 25 °C, a confining pressure of 45 MPa, and a pore pressure of 18 MPa. The sample was kept under pressure for at least 24 h to restore the pressure state close to natural and to relax stresses and reduce the likelihood of creep. The selected pore pressure was equal to the actual bedding conditions, and the confining pressure was slightly below natural in order to minimize the effect of

creep on permeability. Studies [22,23] have shown that rocks have stress memory, which means that repeated application of a load lower than or equal to the previous load reduces the likelihood of irreversible deformations and creep.

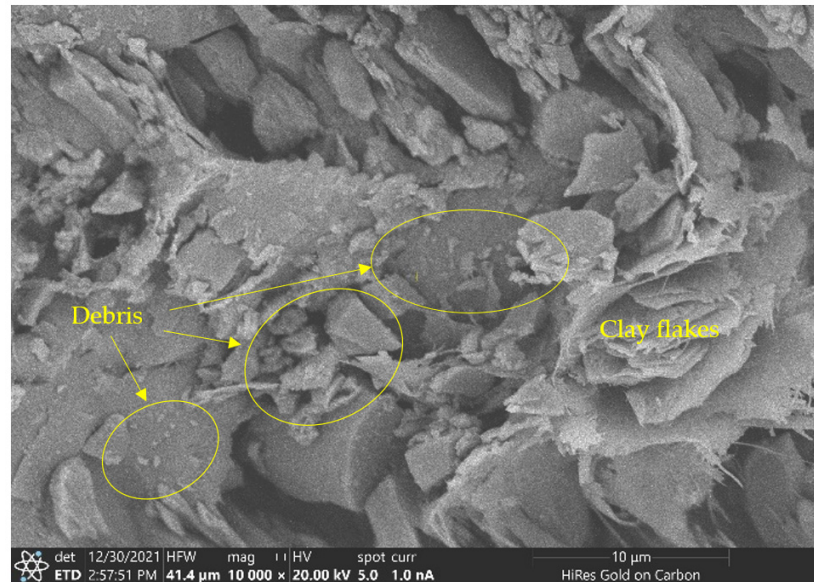


Figure 5. SEM photo of sample 2.

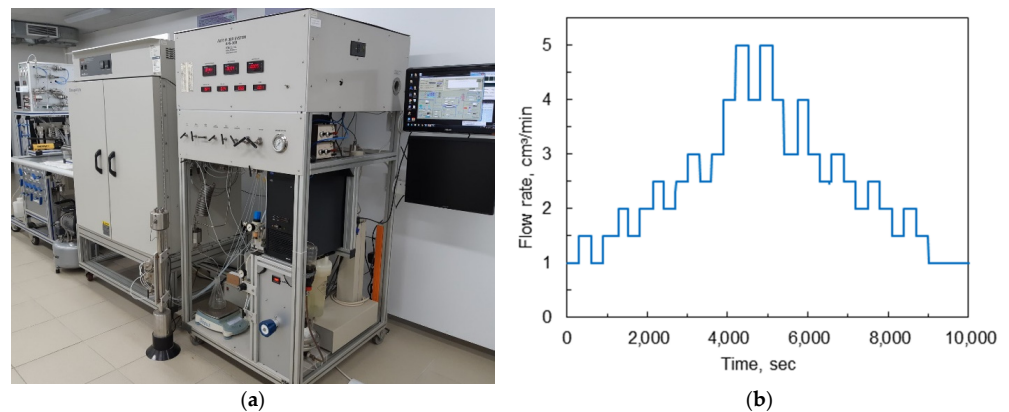


Figure 6. AFS 300 coreflood apparatus (a) and coreflooding test program (b).

Coreflooding was carried out parallel to the rock layers. The fluid was injected with a cyclic flow rate at a constant confining pressure in order to bring the test conditions closer to real ones, when the flow rate can change periodically. The injection program is shown in Figure 6b. The injection rate varied stepwise from 1 to 5 cm³/min; each injection rate lasted for about 5 min. The whole injection cycle lasted about 2–3 h depending on sample permeability.

During injection, pore pressure was defined as the average between the injection pressure and the outlet pressure. A change in injection rate led to a change in pressure drop (ΔP) and pore pressure, but in order to avoid destructive effects, pore pressure and pressure drop should change insignificantly. During flooding of samples 2, 3, and 4, the maximum pressure drop was insignificant and varied from 0.08 to 0.35 MPa. For comparison, in sample 1, which has a lower permeability, the pressure drop was up to 4.3 MPa.

In AFS 300 data from pressure sensors at the inlet and outlet of the sample, as well as from flow sensors, were recorded at a frequency of one measurement per 3 s. Based on the obtained data on the flow rate (q) and the pressure drop (ΔP), and based on the viscosity of

the fluid (μ), length (L), and area (S) of the sample, the instantaneous permeability (k) was determined by the Darcy's formula:

$$k = \frac{\mu \cdot q \cdot L}{\Delta P \cdot S} \quad (2)$$

The calculated instantaneous permeability values were filtered using the MATLAB software. Plots for relative permeability (k/k_o , where k is instantaneous permeability, k_o is initial permeability) from the effective pressure (P_{eff}) and amount of injected fluid, expressed in the number of pore volumes (V/V_p , where V is the volume of the injected fluid in cm^3 , V_p is the volume of the pore space of the sample) were plotted.

During coreflooding, the injection rate (q) was used as a control parameter, and since the samples used have different porosity and permeability, for a comparative assessment, the average velocity (v) of the fluid through the core samples was used, which was determined by the formula:

$$v = \frac{q}{m \cdot S} \quad (3)$$

where m is porosity, S is area of the sample.

Data on maximum flow, pressure drop, injection rate, fluid used, and porosity change are presented in Table 3.

Table 3. Coreflooding conditions and calculated values of the coefficients of Equation (1).

Sample №	1	2	3	4
Max flow rate, mL/min	0.75	5	2.5	2.5
ΔP , MPa	4.3	0.14	0.08	0.35
v , m/day	19	100	60	61
Fluid	Deionized water	Kerosene	Kerosene	Deionized water
ΔK_{por}	+5.76%	+0.2%	+0.1%	+0.5%
a	-	0.033	0.116	0.127
b	-	-0.073	-0.135	0.221
c	-	-0.00033	-0.00081	-0.00212
d	-	0.968	0.842	0.782
R^2	-	0.99	0.99	0.99

3.2. Coreflooding Test Results and Analysis

Finally, it was found that the permeability of all samples decreased during injection (Figure 7). The permeability does not depend on the effective pressure and decreases even with a significant increase in pore pressure, which was especially clearly observed in sample 1 (Figure 7a). Permeability reduction of sample 1 was about 16%. The sample has the lowest permeability and the largest pressure drop—4.3 MPa. Permeability at such a high pressure drop, in addition to the colloid migration, could be influenced by damaging effects, as evidenced by a comparative computed tomography (Figure 8).

During injection with a small change in the effective pressure, for samples 2, 3, and 4, the permeability has a clear dependence on the injected volume (Figure 7b). Curve fitting analysis showed that the change in the permeability of the samples is described with high accuracy by Equation (1), and the calculated values of the equation coefficients are presented in Table 3.

For samples 2 and 3, which have approximately the same properties, the decrease in permeability was 10 and 25%, respectively. This difference is due to the greater layered heterogeneity of sample 2 compared to sample 3. In both samples, kerosene was injected.

The largest decrease in permeability is observed in sample 4—more than 50% (Figure 7). This is due to the injection of deionized water, which chemically interacts with clay minerals and pyrite, which are contained in small amounts in the samples. Interaction of deionized water with clay particles can lead to their dispersion, migration and the blocking of pores; pyrite can interact with deionized water and form insoluble colloids of iron hydroxide 3.

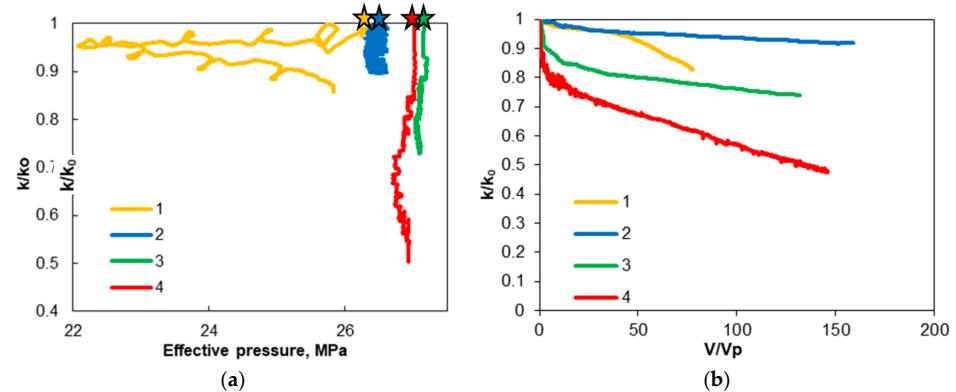


Figure 7. Dynamics of relative permeability on effective pressure (a) and injected volume (b) during coreflooding. The numbers correspond to the sample numbers. The stars correspond to the initial permeability values.

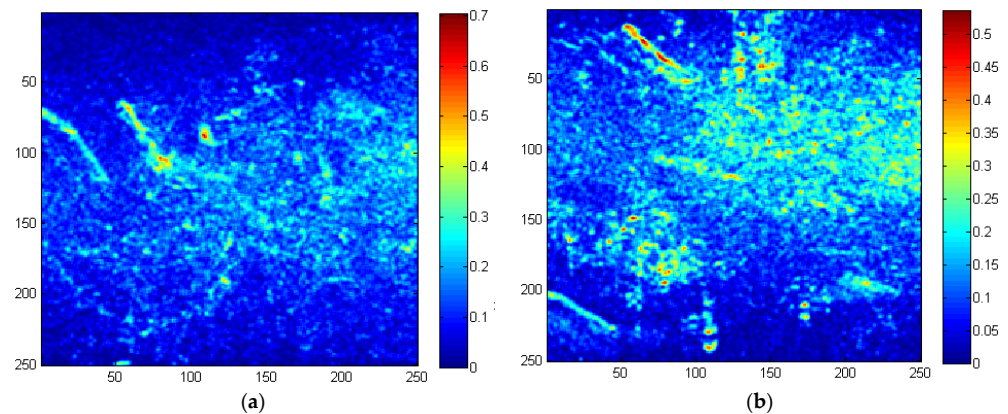


Figure 8. Pore space map of sample 1. Colour bar shows the accumulated crack opening, mm, (a) before coreflooding test; (b) after coreflooding test (the direction of fluid movement during filtration is from right to left). Pore space map is built for clarity, the selected face is parallel to the prevailing crack opening. The faces before and after coreflooding may not match.

3.3. CT Results and Analysis

During computed tomography, images of the void space and fracture maps (Figure 8) of the samples were obtained before and after coreflooding and the quantitative change in the void space were determined. Comparative tomography showed that in sample 1 there is the largest increase in porosity (ΔK_{por}) by almost 6%; in other samples, the porosity changed within the error and ranges from 0.1 to 0.5% (Table 3). The reason for such a large change in the structure of the pore space in sample 1 is most likely a large pressure drop during coreflooding.

The void images and fracture maps made it possible to highlight the main features of the change in the void space of sample 1 after coreflooding:

- the increase in the crack opening mainly in the central part of the sample, probably due to the wedging action of a high pressure drop up to 4.3 MPa;
- the closing of cracks emerging on the surface of the sample due to the influence of internal wedging and external confining pressures;
- due to the relatively low resolution (20.1 μm), the analysis of the influence of the migration of particles and colloids with a size of up to 20 μm was not possible.

4. Discussion and Model Explanation

The main objective of research was to establish the cause of the hysteresis in the permeability of porous low-clay media with minor changes in effective pressure. For this, sandstone samples with a clay content of up to 2% were used.

The studies showed that the permeability of the cores decreases when the fluid moves inside the samples, which is evidenced by a clear dependence of permeability on the volume of fluid injected. This suggests that when the fluid moves, the pores are blocked, and this can occur due to the presence of natural colloids, the presence of which was confirmed by the analysis of SEM photographs of rock samples (Figure 5).

The coreflooding program implied a stepwise change in the injection rate, as shown by numerous studies [24–46]. A change in the injection rate leads to the release of colloids, which can be located on the walls of the pores, strained at pore throats, bridge clogged, and lying in stagnant zones. The release of colloids is evidenced by a change in the concentration of colloids in the effluent washed out from the porous medium, a change in the geometry of the pore space, and a change in hydraulic conductivity–permeability. In our case, we judge the migration of colloids by the decrease in the permeability of samples during injection of a pure liquid with varying flow rates.

Injection of a large volume of fluid with fluctuated rates can lead not only to colloid migration and pore clogging, but also to pore unclogging and washout of colloids from the rock. Washout of colloids will naturally lead to an increase in rock permeability. When colloids are washed out, it is expected that the permeability initially decreases and then increases [24]. In this case, the washout rate will depend on the injection rate, the size of the particles and pore channels, as well as the size of the core sample. Washout of particles from media with high porosity and permeability can occur within several hours of filtration; in [24], using the soil model as an example, it was shown that an increase in fluid flow rather quickly leads to the washout of free particles and an increase in the permeability of the medium. In media with low porosity and permeability, colloids can be washed out for quite a long time, so, using the example of [34], it is shown that even with small sizes of core samples that are 4 mm long, the permeability decreases within more than 8 h of injection. In our case, the decrease in permeability occurred constantly throughout the injection, which indicates a fairly large number of colloids and a low speed of their movement [33,34].

Figure 9 shows the scheme of pore channels blocking during the migration of colloids. In the initial period, relatively small pore channels are blocked by colloids and the permeability decreases exponentially until all small pores are blocked, and only those channels in which there are no conditions for bridge clogging at given flow rates and colloid concentrations will participate in filtration. Mathematically, in Equation (1) the proportion of residual permeability is described by the coefficient d . Residual permeability is the permeability at which the conductivity of the porous medium is due to channels in which there is no possibility of bridging under current flow conditions.

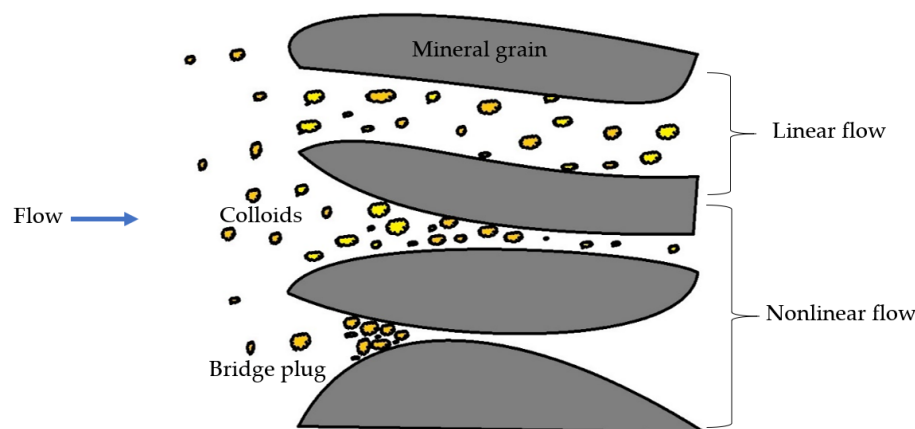


Figure 9. Scheme of pore channels blocking during the migration of colloids.

The analytical equation of permeability (1) shows that in the initial period, the permeability decreases non-linearly according to an exponential law, and then decreases almost linearly or stabilizes (Figures 4c and 7b). The physical meaning of the exponential component of Equation (1) can be described by pore blocking due to bridging [35,36]. With a large

proportion of small channels, the exponential component becomes more significant, and the larger the size of pore channels in the medium, the slower the decrease in hydraulic conductivity.

The presence of even a small number of highly conductive channels will contribute to a smaller decrease in the apparent permeability of the samples due to bridging, since the contribution of such channels to the apparent permeability is high, and the decrease in their conductivity is minimal. The presence of highly conductive pore channels is expressed in a larger value of the residual permeability and the coefficient d of Equation (1). According to the CT of samples 2 and 3, it can be seen that sample 2, with almost equal permeability, has a zone with increased pore opening (Figure 10), which causes a smaller decrease in permeability in the initial period of injection and a relatively large value of the coefficient d of Equation (1) (Table 3).

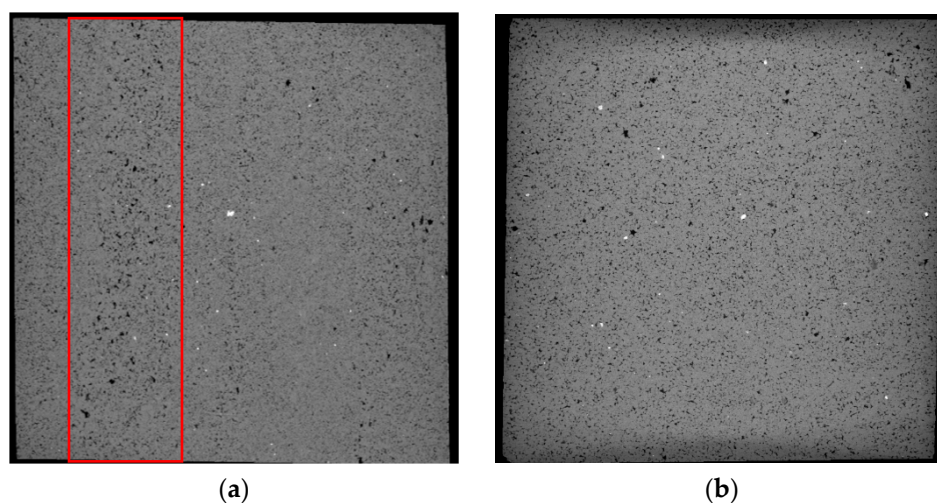


Figure 10. CT scan of samples 2 (a) and 3 (b). Density shown in gray gradient. The zone with increased porosity is marked with a red rectangle. Voids shown in black, matrix in grayscale.

The linear component of Equation (1) describes a further linear decrease in permeability, which occurs due to the migration of colloids and their detachment and attachment to the pore walls [37]. Any violation of the equilibrium state of the fluid flow can lead to the release of colloids and their further migration. Over time, sufficiently large channels can be bridge clogged as the number of colloids attached to the pore channel wall increases [30].

5. Conclusions

The closure of microcracks leads to a decrease in permeability, but this only occurs at large values of effective pressure change, from several units to tens of MPa. In reservoir conditions, such a change in effective pressure corresponds to almost complete depletion; however, as an analysis of the well test data from C_{1tl} terrigenous reservoir showed, a decrease in permeability and its hysteresis are also manifested with smaller fluctuations in reservoir and effective pressures in the early stages of oil production. In this regard, mechanical models that take into account the presence of a threshold for opening microcracks and creep are not suitable for predicting permeability.

Based on the analysis of well test data from the C_{1tl} terrigenous reservoir, a permeability model was obtained that takes into account the amount of oil produced from the well. The model is applicable only in the initial period of oil production under conditions that exclude the influence of other factors, such as relative phase permeability due to water and gas breakthrough to the well, and creep and precipitation as a result of chemical reactions.

Coreflooding tests according to the method proposed by us with varying injection rates showed a significant degradation of the porous media permeability. The model proposed on the basis of well test data showed high convergence with the results of coreflooding. The proposed model can be used to predict changes in reservoir permeability and well flow

rates in the initial period of oil production. A detailed study of the structure of the pore space showed that the main reason for the decrease in the permeability of low-clay rocks in the initial period of production is the migration of natural colloids.

Author Contributions: Conceptualization, E.V.K. and E.P.R.; methodology, E.V.K.; software, E.V.K.; validation, M.S.T., E.P.R. and M.A.G.; formal analysis, H.J.; investigation, E.A.G.; resources, V.V.P.; data curation, E.A.G.; writing—original draft preparation, E.V.K.; writing—review and editing, E.V.K. and E.P.R.; visualization, V.V.P.; supervision, H.J.; project administration, M.S.T. and M.A.G.; funding acquisition, V.V.P. All authors have read and agreed to the published version of the manuscript.

Funding: This research was funded by Russian Science Foundation, grant number 22-19-00447, <https://rscf.ru/project/22-19-00447/> (accessed on 8 July 2022).

Institutional Review Board Statement: Not applicable.

Informed Consent Statement: Not applicable.

Data Availability Statement: The datasets analyzed during the current study are available from the corresponding author on reasonable request.

Conflicts of Interest: The authors declare no conflict of interest.

References

- Nur, A.; Byerlee, J.D. An exact effective stress law for elastic deformation of rock with fluids. *J. Geophys. Res. Space Phys.* **1971**, *76*, 6414–6419. [[CrossRef](#)]
- Li, M.; Bernabé, Y.; Xiao, W.-I.; Chen, Z.-Y.; Liu, Z.-Q. Effective pressure law for permeability of E-bei sandstones. *J. Geophys. Res. Space Phys.* **2009**, *114*, B07205. [[CrossRef](#)]
- Ghabezloo, S.; Sulem, J.; Guédon, S.; Martineau, F. Effective stress law for the permeability of a limestone. *Int. J. Rock Mech. Min. Sci.* **2009**, *46*, 297–306. [[CrossRef](#)]
- Sigal, R.F. The pressure dependence of permeability. *Petrophys. SPWLA J. Form. Eval. Reserv. Descr.* **2002**, *43*, 92–102.
- Kozhevnikov, E.; Riabokon, E.; Turbakov, M. A model of reservoir permeability evolution during oil production. *Energies* **2021**, *14*, 2695. [[CrossRef](#)]
- Kozhevnikov, E.V.; Turbakov, M.S.; Riabokon, E.P.; Poplygin, V.V. Effect of effective pressure on the permeability of rocks based on well testing results. *Energies* **2021**, *14*, 2306. [[CrossRef](#)]
- Pourciau, R.D.; Fisk, J.H.; Descant, F.J.; Waltman, B. Completion and Well Performance Results, Genesis Field, Deepwater Gulf of Mexico. *SPE Drill. Complet.* **2005**, *20*, 147–155. [[CrossRef](#)]
- Kwon, O.; Kronenberg, A.K.; Gangi, A.F.; Johnson, B. Permeability of Wilcox shale and its effective pressure law. *J. Geophys. Res. Space Phys.* **2001**, *106*, 19339–19353. [[CrossRef](#)]
- Zheng, J.; Zheng, L.; Liu, H.-H.; Ju, Y. Relationships between permeability, porosity and effective stress for low-permeability sedimentary rock. *Int. J. Rock Mech. Min. Sci.* **2015**, *78*, 304–318. [[CrossRef](#)]
- David, C.; Menendez, B.; Zhu, W.; Wong, T.F. Mechanical compaction, microstructures and permeability evolution in sandstones. *Phys. Chem. Earth A* **2001**, *26*, 45–51. [[CrossRef](#)]
- Zhang, Y.; Wang, L.; Li, H.; Zhang, Y.; Fu, G. Experimental study of the permeability of fractured sandstone under complex stress paths. *Energy Sci. Eng.* **2020**, *8*, 3217–3227. [[CrossRef](#)]
- Zhang, D.M.; Yang, Y.S.; Chu, Y.P.; Zhang, X.; Xue, Y.G. Influence of loading and unloading velocity of confining pressure on strength and permeability characteristics of crystalline sandstone. *Results Phys.* **2018**, *9*, 1363–1370. [[CrossRef](#)]
- Selvadurai, A.P.S.; Zhang, D.; Kang, Y. Permeability evolution in natural fractures and their potential influence on loss of productivity in ultra-deep gas reservoirs of the Tarim Basin, China. *J. Nat. Gas Sci. Eng.* **2018**, *58*, 162–177. [[CrossRef](#)]
- Mavko, G.; Jizba, D. Estimating grain-scale fluid effects on velocity dispersion in rocks. *Geophysics* **1991**, *56*, 1940–1949. [[CrossRef](#)]
- Liu, H.-H.; Rutqvist, J.; Berryman, J.G. On the relationship between stress and elastic strain for porous and fractured rock. *Int. J. Rock Mech. Min. Sci.* **2009**, *46*, 289–296. [[CrossRef](#)]
- Dong, J.-J.; Hsu, J.-Y.; Wu, W.-J.; Shimamoto, T.; Hung, J.-H.; Yeh, E.-C.; Wu, Y.-H.; Sone, H. Stress-dependence of the permeability and porosity of sandstone and shale from TCDP Hole-A. *Int. J. Rock Mech. Min. Sci.* **2010**, *47*, 1141–1157. [[CrossRef](#)]
- An, C.; Killough, J.; Xia, X. Investigating the effects of stress creep and effective stress coefficient on stress-dependent permeability measurements of shale rock. *J. Pet. Sci. Eng.* **2021**, *198*, 108155. [[CrossRef](#)]
- Pittman, E.D.; Larese, R.E. Compaction of Lithic Sands: Experimental Results and Applications (1). *AAPG Bull.* **1991**, *75*, 1279–1299. [[CrossRef](#)]
- Hu, C.; Agostini, F.; Skoczylas, F.; Jeannin, L.; Egermann, P.; Jia, Y. Transport property evolution during hydrostatic and triaxial compression of a high porosity sandstone. *Eur. J. Environ. Civ. Eng.* **2020**, 1–14. [[CrossRef](#)]
- Hu, C.; Agostini, F.; Jia, Y. Porosity and Permeability Evolution with Deviatoric Stress of Reservoir Sandstone: Insights from Triaxial Compression Tests and In Situ Compression CT. *Geofluids* **2020**, *2020*, 6611079. [[CrossRef](#)]

21. Li, X.; Chen, Y.F.; Wei, K.; Hu, R.; Yang, Z.B. A threshold stresses-based permeability variation model for microcracked porous rocks. *Eur. J. Environ. Civ. Eng.* **2020**, *24*, 787–813. [[CrossRef](#)]
22. Pimienta, L.; Quintal, B.; Caspari, E. Hydro-mechanical coupling in porous rocks: Hidden dependences to the microstructure? *Geophys. J. Int.* **2021**, *224*, 973–984. [[CrossRef](#)]
23. Wang, C.; Wang, R.; Huo, Z.; Xie, E.; Dahlke, H.E. Colloid transport through soil and other porous media under transient flow conditions—A review. *Wiley Interdiscip. Rev. Water* **2020**, *7*, e1439. [[CrossRef](#)]
24. Chen, W.; Han, Y.; Agostini, F.; Skoczylas, F.; Corbeel, D. Permeability of a Macro-Cracked Concrete Effect of Confining Pressure and Modelling. *Materials* **2021**, *14*, 862. [[CrossRef](#)]
25. Mayr, S.I.; Stanchits, S.; Langenbruch, C.; Dresen, G.; Shapiro, S.A. Acoustic emission induced by pore-pressure changes in sandstone samples. *Geophysics* **2011**, *76*, MA21–MA32. [[CrossRef](#)]
26. Pestman, B.J.; Van Munster, J.G. An acoustic emission study of damage development and stress-memory effects in sandstone. *Int. J. Rock Mech. Min. Sci. Geomech. Abstr.* **1996**, *33*, 585–593. [[CrossRef](#)]
27. Yang, J.; Yin, Z.-Y.; Laouafa, F.; Hicher, P.-Y. Analysis of suffusion in cohesionless soils with randomly distributed porosity and fines content. *Comput. Geotech.* **2019**, *111*, 157–171. [[CrossRef](#)]
28. Bedrikovetsky, P.; Siqueira, F.D.; Furtado, C.A.; Souza, A.L.S. Modified particle detachment model for colloidal transport in porous media. *Transp. Porous Med.* **2011**, *86*, 353–383. [[CrossRef](#)]
29. Gruesbeck, C.; Collins, R.E. Entrainment and deposition of fine particles in porous media. *Soc. Pet. Eng. J.* **1982**, *22*, 847–856. [[CrossRef](#)]
30. Muecke, T.W. Formation fines and factors controlling their movement in porous media. *J. Pet. Technol.* **1979**, *31*, 144–150. [[CrossRef](#)]
31. Khilar, K.C.; Fogler, H.S. Colloidally induced fines migration in porous media. *Rev. Chem. Eng.* **1987**, *4*, 41–108. [[CrossRef](#)]
32. Parvan, A.; Jafari, S.; Rahnema, M.; Norouzi-Apourvari, S.; Raoof, A. Insight into particle detachment in clogging of porous media; a pore scale study using lattice Boltzmann method. *Adv. Water Resour.* **2021**, *151*, 103888. [[CrossRef](#)]
33. Klimenko, L.S.; Maryshev, B.S. Numerical simulation of microchannel blockage by the random walk method. *Chem. Eng. J.* **2020**, *381*, 122644. [[CrossRef](#)]
34. Frey, J.M.; Schmitz, P.; Dufreche, J.; Gohr Pinheiro, I. Particle deposition in porous media: Analysis of hydrodynamic and weak inertial effects. *Transp. Porous Media* **1999**, *37*, 25–54. [[CrossRef](#)]
35. Borazjani, S.; Behr, A.; Genolet, L.; Van Der Net, A.; Bedrikovetsky, P. Effects of fines migration on low-salinity waterflooding: Analytical modelling. *Transp. Porous Med.* **2017**, *116*, 213–249. [[CrossRef](#)]
36. Yang, Y.; You, Z.; Siqueira, F.D.; Vaz, A.; Bedrikovetsky, P. Modelling of slow fines migration and formation damage during rate alteration. In Proceedings of the SPE Asia Pacific Oil & Gas Conference and Exhibition, Perth, Australia, 25–27 October 2016. [[CrossRef](#)]
37. Ochi, J.; Vernoux, J.-F. Permeability decrease in sandstone reservoirs by fluid injection. *J. Hydrol.* **1998**, *208*, 237–248. [[CrossRef](#)]
38. Chen, C.; Packman, A.I.; Gaillard, J.-F. Pore-scale analysis of permeability reduction resulting from colloid deposition. *Geophys. Res. Lett.* **2008**, *35*, L07404. [[CrossRef](#)]
39. Sauret, A.; Somszor, K.; Villermaux, E.; Dressaire, E. Growth of clogs in parallel microchannels. *Phys. Rev. Fluids* **2018**, *3*, 104301. [[CrossRef](#)]
40. Qiu, K.; Gherryo, Y.; Shatwan, M.; Fuller, J.; Martin, W. Fines migration evaluation in a mature field in Libya. In Proceedings of the SPE Asia Pacific Oil and Gas Conference and Exhibition, Perth, Australia, 20–22 October 2008. [[CrossRef](#)]
41. Ramachandran, V.; Fogler, H.S. Plugging by hydrodynamic bridging during flow of stable colloidal particles within cylindrical pores. *J. Fluid Mech.* **1999**, *385*, 129–156. [[CrossRef](#)]
42. Torkzaban, S.; Bradford, S.A.; Vanderzalm, J.L.; Patterson, B.M.; Harris, B.; Prommer, H. Colloid release and clogging in porous media: Effects of solution ionic strength and flow velocity. *J. Contam. Hydrol.* **2015**, *181*, 161–171. [[CrossRef](#)]
43. Kozhevnikov, E.V.; Turbakov, M.S.; Gladkikh, E.A.; Riabokon, E.P.; Poplygin, V.V.; Guzev, M.A.; Qi, C.; Kunitskikh, A.A. Colloid Migration as a Reason for Porous Sandstone Permeability Degradation during Coreflooding. *Energies* **2022**, *15*, 2845. [[CrossRef](#)]
44. Kozhevnikov, E.V.; Turbakov, M.S.; Gladkikh, E.A.; Riabokon, E.P.; Poplygin, V.V.; Guzev, M.A.; Qi, C.; Jing, H. Colloidal-induced permeability degradation assessment of porous media. *Géotech. Lett.* **2022**, *12*, 1–18. [[CrossRef](#)]
45. Xiao, B.; Wang, W.; Zhang, X.; Long, G.; Fan, J.; Chen, H.; Deng, L. A novel fractal solution for permeability and Kozeny-Carman constant of fibrous porous media made up of solid particles and porous fibers. *Powder Technol.* **2019**, *349*, 92–98. [[CrossRef](#)]
46. Liang, M.; Fu, C.; Xiao, B.; Luo, L.; Wang, Z. A fractal study for the effective electrolyte diffusion through charged porous media. *Int. J. Heat Mass Transf.* **2019**, *137*, 365–371. [[CrossRef](#)]